AD-A150 904 THUNDERSTORM PHENOMENA AND WEATHER RADAR SCANNING STRATEGIES(U) NATIONAL OCEANIC AND ATMOSPHERIC ADMINISTRATION NORMAN OK NAT.. S VASILOFF ET AL. 1/1

UNCLASSIFIED DEC 84 DOT/FAA/PM-85/14 DTFA01-80-Y-10524 F/G 4/2 NL

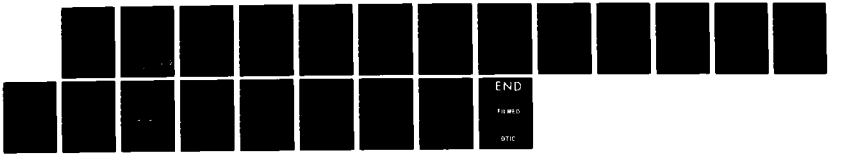

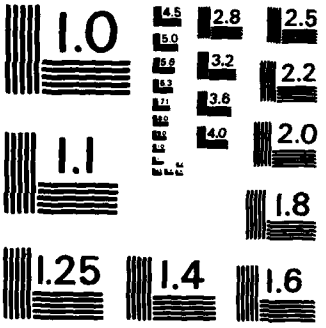

MICROCOPY RESOLUTION TEST CHART
NATIONAL BUREAU OF STANDARDS-1963-A

(3)

DOT/FAA/PM-85-14

Program Engineering
and Maintenance Service
Washington, D.C. 20591

Thunderstorm Phenomena and Weather Radar Scanning Strategies

AD-A158 904

Steven Vasiloff
Michael Istok
R.J. Doviak

U.S. Department of Commerce
National Severe Storms Laboratory
1313 Halley Circle
Norman, Oklahoma 73069

December 1984

Final Report

This Document is available to the public
through the National Technical Information
Service, Springfield, Virginia 22161.

DTIC FILE COPY

DTIC
ELECTE
SEP 6 1985
S D
B

U.S. Department of Transportation
Federal Aviation Administration

85 9 03 026

This document is disseminated under the sponsorship of the U.S. Department of Transportation in the interest of information exchange. The United States Government assumes no liability for its contents or use thereof.

Technical Report Documentation Page

1. Report No.	2. Government Accession No.	3. Recipient's Catalog No.
DOT/FAA/PM-85/14	AD-A158 904	

4. Title and Subtitle	5. Report Date
Thunderstorm Phenomena and Weather Radar Scanning Strategies	December 1984
	6. Performing Organization Code
	8. Performing Organization Report No.
7. Author(s)	
Steve Vasiloff, Michael Istok, R.J. Doviak	
9. Performing Organization Name and Address	10. Work Unit No. (TRAIS)
U.S. Dept. of Commerce National Oceanic & Atmospheric Administration National Severe Storms Laboratory	11. Contract or Grant No. DTFA01-80-Y-10524
	13. Type of Report and Period Covered
12. Sponsoring Agency Name and Address	
U.S. Dept. of Transportation Federal Aviation Administration 800 Independence Ave., SW Washington, D.C. 20591	Final Report
	14. Sponsoring Agency Code FAA/APM-310

15. Supplementary Notes
Prepared under Interagency Agreement DTFA01-80-Y-10524 as amended, managed by the Primary Radar Program APM-310

16. Abstract

Examination of several thunderstorm cells' maximum reflectivity and updraft speed shows that growth rates of maximum reflectivity factor ranged from 4 to 7 dBZ min^{-1} and those of maximum updraft speed ranged from 3 to 7 m s^{-1} min^{-1}. Times of occurrence of maximum values of reflectivity, storm height, and updraft speed are compared. The Air Force Geophysics Laboratory's storm analysis and tracking algorithms are used to evaluate interlaced and contiguous (non-interlaced) scanning strategies. Eleven cell attributes are determined and compared for each strategy. The differences between attribute values obtained from successive contiguous scans are about the same as the differences between values obtained from interlaced and contiguous scans for the same time period. Thus, an interlaced scanning strategy may allow detection of some hazards (e.g., low altitude shear) in one-half the time expected using the proposed NEXRAD contiguous scanning strategy without significantly compromising the evaluation of storm attributes. Although these findings are incomplete because of the small data sample they suggest that the NEXRAD radar can provide more timely warnings of low altitude weather hazards in the terminal area if an interlaced scan strategy is used.

17. Key Words	18. Distribution Statement
Growth rates, scanning strategies, Doppler radar, weather hazards, NEXRAD	Document is available to the U.S. public through the National Technical Service, Springfield, VA 22161.

19. Security Classif. (of this report)	20. Security Classif. (of this page)	21. No. of Pages	22. Price
Unclassified	Unclassified	20	

Form DOT F 1700.7 (8-72) Reproduction of completed page authorized

TABLE OF CONTENTS

Technical Report Documentation Page.....i

Table of Contents.....ii

List of Illustrations.....iii

List of Tables.....iv

Preface.....v

1. Introduction.....1

2. Growth Rates of Reflectivity and Updrafts.....2

3. Results.....3

4. Effects of Interlaced Scans on Real-Time Algorithms Used to Track Storm Cells and Determine Their Parameters.....7

5. Summary and Discussion.....9

References.....13

LIST OF ILLUSTRATIONS

Figure 1 Storm-relative horizontal wind and reflectivity factor fields at 1956 CST: (a) 2-km and (b) 9-km levels. The origin of the plot is at the Norman radar site. Updraft regions greater than 10 m s^{-1} are stippled and a scaled velocity vector of 20 m s^{-1} is drawn in the upper right corner. Reflectivity factor is contoured every 10 dBZ. Lines AB and CD give locations of vertical cross sections shown in Fig. 2. The dashed lines outline the approximate areas of cells C0 and C1 at these heights.

Figure 2 Vertical cross sections through cell complex at 1956 showing the reflectivity factor field and the velocity vectors projected onto the plane of the figure. (a) Cross section parallel to cell motion. (b) Cross section parallel to storm motion.

Figure 3 The evolution of (a) Maximum updraft speed (m s^{-1}), and (b) Maximum reflectivity factor (dBZ) at each altitude in cell C1.

Figure 4 As in Fig. 3 except for cell C2.

Figure 5 As in Fig. 3 except for cell C3.

Figure 6 As in Fig. 3 except for cell C4.

Figure 7 Simulation of interlaced azimuthal scans by deletion of alternate ones at constant elevation from the contiguous set.

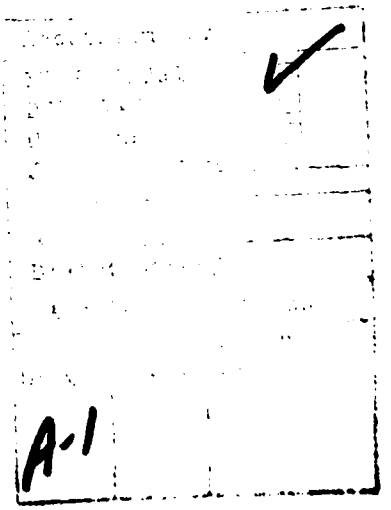

LIST OF TABLES

Table 1. Storm cell attribute values and differences between them, for one interlaced and three non-interlaced scanning strategies.....9

Table 2. Storm cell attributed values, and differences between them, for three interlaced and three non-interlaced scanning strategies.....11

PREFACE

We would like to thank Messrs. Jean Lee and Don Burgess for their critical review, Ms. Joan Kimpel and Mr. Robert Goldsmith who performed the graphics, and Ms. Michelle Foster who typed the manuscript.

1. INTRODUCTION

The NEXRAD radars (as proposed) will scan azimuthally at increasing elevation angles to survey storm volumes in about 5 minutes to detect and track weather phenomena (e.g., tornadoes, wind shear, intense rain) hazardous to life and property. Because aircraft at low altitudes are particularly vulnerable to wind shear during approach and departure at airports, there is concern that the 5-minute volume scan update rate is too slow for weather hazards to be detected in time for the pilot to take corrective action. Added to the time interval between passes of the radar beam through the region of the incipient hazard is the time required to process the Doppler data to decide whether a hazard exists (real-time computer-based algorithms are being developed to issue alerts), the time to communicate an alert to an affected aircraft, and the time it takes for the pilot and aircraft to respond to avoid the hazard or to take other corrective action.

Not only is it important to detect weather hazards, it is equally important to determine hazard potential. Usually hazards are small-scale events embedded in larger-scale weather systems that are more easily detected and monitored. For example, the NEXRAD radar cannot resolve tornadoes at all operating ranges but can easily resolve the mesocyclones from which tornadoes often evolve. Radar siting determines resolution and coverage of weather hazards in the terminal area, and Mahapatra, et al. (1983) have presented arguments for locating the radar in the terminal area.

Although a storm's peak reflectivity is commonly used to gauge the severity of thunderstorms (i.e., likelihood of hail or strong winds), and reflectivity patterns can sometimes indicate the presence of tornadic circulations, warnings based on reflectivity structure alone have serious shortcomings. For example, researchers and radar meteorologists have found (JDOP, 1979) that false alarm ratios (FAR) are as high as 0.79 for tornado warnings based on reflectivity structure alone. Because the NEXRAD radar has much finer spatial resolution than the present weather radars, and is capable of measuring both reflectivity and the radial component of wind, there are better chances to detect or predict the hazardous event, and thus give more accurate warnings (e.g., the FAR of 0.79 was reduced to 0.38 when Doppler radar was used).

On the other hand, neither the NEXRAD radar nor any other will have perfect capability for hazard detection because its resolution is finite and a

finite time elapses during surveillance of the tremendous volume of space in which the hazard may lurk. The 5-minute update rate may be too long to detect hazards whose lifetimes may not be much longer, and there may be need to monitor, more frequently, volumes of space that may contain these incipient hazards. For example, typical horizontal dimensions of microbursts are 1 to 3 km and lifetimes range from 5 to 15 minutes, whereas the period of severe wind shear in the microburst lasts from 2 to 4 minutes with an average velocity difference of 25 m s^{-1} across the divergent flow (McCarthy and Serafin, 1984). An interlaced scanning strategy has been proposed to provide more frequent sampling of some weather hazards, especially low-altitude shear (Mahapatra and Zrnic', 1983).

There are two approaches that can be followed to halve the time to detect hazards or potentially hazard-causing phenomena: (1) double the scan rate or (2) use interlaced scans. Assuming that the scale of the hazard-causing phenomenon is larger than the spacings between elevation-angle increments, either strategy would serve to detect the phenomenon, however the interlaced scanning strategy is more easily accomplished. On the other hand, gaps in height coverage during one of the interlaced-scan pairs could compromise timely detection of the hazard: its size being too small to be adequately sampled by at least two contiguous (in elevation) azimuthal sweeps of the beam. However, if the phenomenon is hazardous only in limited regions, for example low-altitude shear, an extra sweep at low elevation angles is all that may be required to scan more frequently those regions most likely to harbor hazards.

The purpose of this report is to examine the effects that interlaced scans have on accuracy and reliability of some of the NEXRAD storm analysis and tracking algorithms and to determine the growth rates of some storm phenomena.

2. GROWTH RATES OF REFLECTIVITY AND UPDRAFTS (19 JUNE 1980)

This study examines reflectivity and updraft growth rates in cells of a storm that evolved from a group of small cells into a supercell thunderstorm (Vasiloff and Brandes, 1984).

The subject storm formed in central Oklahoma on 19 June 1980 and was observed with Doppler radars for nearly 2 1/2 hours. Both severe thunderstorm

and tornado warnings were issued by the National Weather Service Forecast Office in Oklahoma City. A total of 21 dual-Doppler volume scans were obtained. Reference times for analysis began at 1942 (all times CST and all heights AGL) and ended at 2215, with a median interval of ~5 minutes between volume scans Three-dimensional wind fields were constructed using a variational procedure that constrains the vertical wind w at ground and storm top to be zero (Ray et al., 1980). The final adjusted w is from a downward integration of an anelastic form of the continuity equation.

Statistics have been developed for four cells within the storm at various times. ("Cell" is defined as a volume of space that has a reflectivity maximum and an updraft, both of which can be identified in consecutive volume scans.) Average cell velocity was from 255° at 9.2 ms^{-1}. Each cell formed on the right flank of the storm, moved through the storm, and dissipated on its left flank giving the storm a motion from 320° at 8.0 m s^{-1}, 65° to the right of cell motion. Diagrams showing the evolution of maximum reflectivity and updraft speed at each height for each cell are presented in Section 3. The diagrams are constructed by plotting maximum values at each level (height separation Δz = 1 km) in the cell versus time. Horizontal and vertical cross sections of wind and reflectivity are shown for only one cell of the complex because the cells are all very similar in structure.

3. RESULTS

Storm-relative horizontal wind and reflectivity factor fields early in the lifetime of the storm are presented in Fig. 1. At 1956, the cell complex comprises two significant cells, C0 and C1, whose reflectivity peaks at the 2-km level are separated by about 7 km (see Fig. 1a). Two reflectivity factor maxima, at (x = -35, y = -13) and (x = -40, y = -10), are found in cell C0 which is in its dissipative stage of evolution. During its mature stage, maximum reflectivity factor was only 32 dBZ, peak updraft speeds approached 10 m s^{-1}, and the maximum height of the cell was ~11 km. Cell C1, now near its mature stage, is stronger; its updraft speeds exceed 10 m s^{-1} at 9 km (Fig. 1b).

Vertical cross sections through the cell complex are given in Fig. 2 . The positions of the cross sections were chosen in order to best illustrate the structure and evolution of the storm and its components. In Figure 2a the updraft in C1 (x = -43 to -48) slopes to the east with height. The reflectivity core is displaced downwind from the updraft center and overlies a

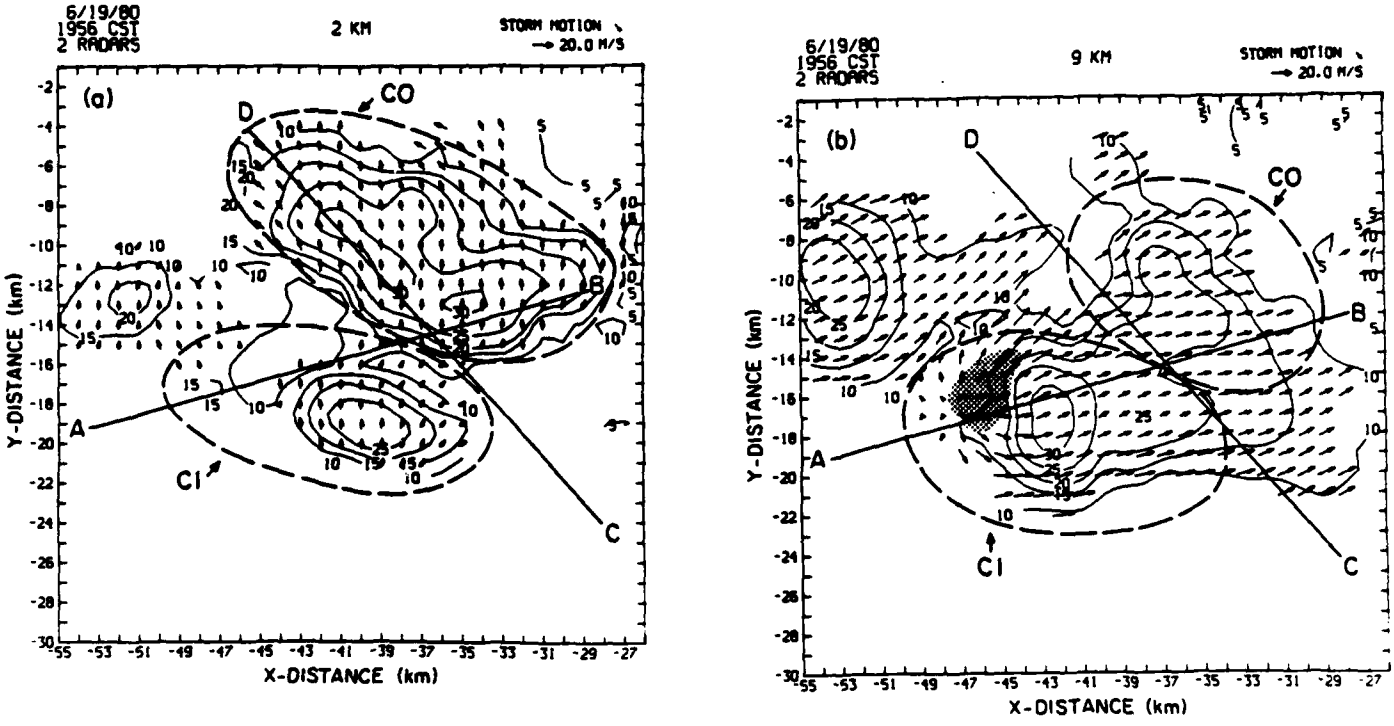

Figure 1 *Storm-relative horizontal wind and reflectivity factor fields at 1956 CST: (a) 2-km and (b) 9-km levels. The origin of the plot is at the Norman radar site. Updraft regions greater than 10 m s^{-1} are stippled and a scaled velocity vector of 20 m s^{-1} is drawn in the upper right corner. Reflectivity factor is contoured every 10 dBZ. Lines AB and CD give locations of vertical cross sections shown in Fig. 2. The dashed lines outline the approximate areas of cells C0 and C1 at these heights.*

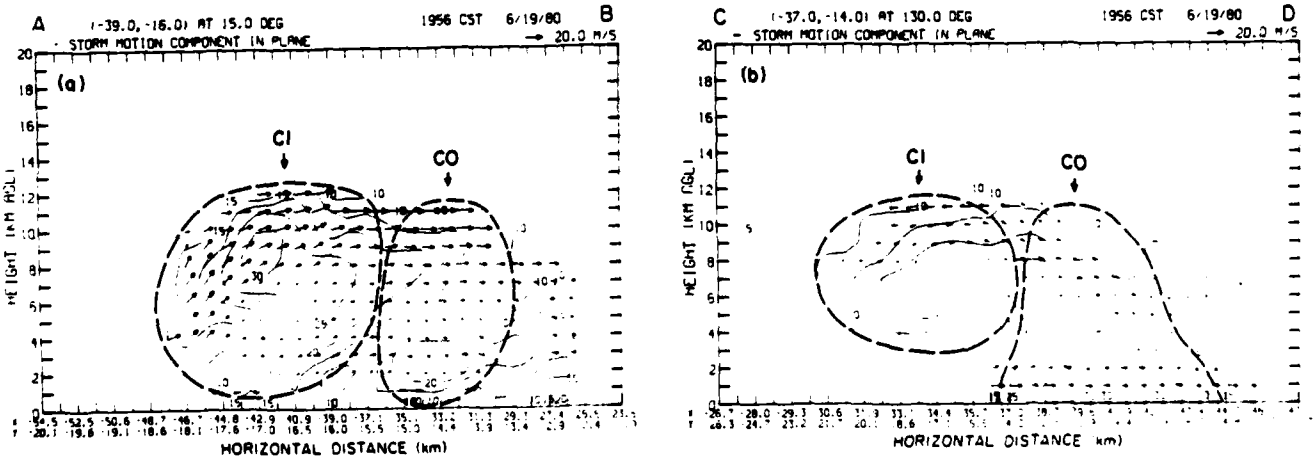

Figure 2 *Vertical cross sections through cell complex at 1956 showing the reflectivity factor field and the velocity vectors projected onto the plane of the figure. (a) Cross section parallel to cell motion. (b) Cross section parallel to storm motion.*

weaker reflectivity region. The 20-dBZ maximum (x = -31 to -35) below the reflectivity overhang in Fig. 2a is part of the dying cell C0. Cross section CD (Fig. 2b) also reveals a reflectivity overhang similar to that of supercell structure. As in Fig. 2a, the developing cell C1 appears aloft in only this cross section.

Diagrams showing the evolution of maximum reflectivity factor and updraft speed at each height in C1 are shown in Fig. 3. C1, which became more intense than its predecessor, C0, first appeared between 6 and 10 km elevation at ~1942. Peak updraft speeds (>25 m s^{-1}) occurred about 7 minutes before the maximum height of the cell (~13 km) and about 20 minutes before maximum reflectivity factor (50 dBZ). The entire life cycle of C1 was completed in about an hour. The maximum reflectivity factor growth rate was ~4 dBZ min^{-1} at low altitudes; the maximum updraft growth rate was ~5 m s^{-1} min^{-1} at middle to high altitudes.

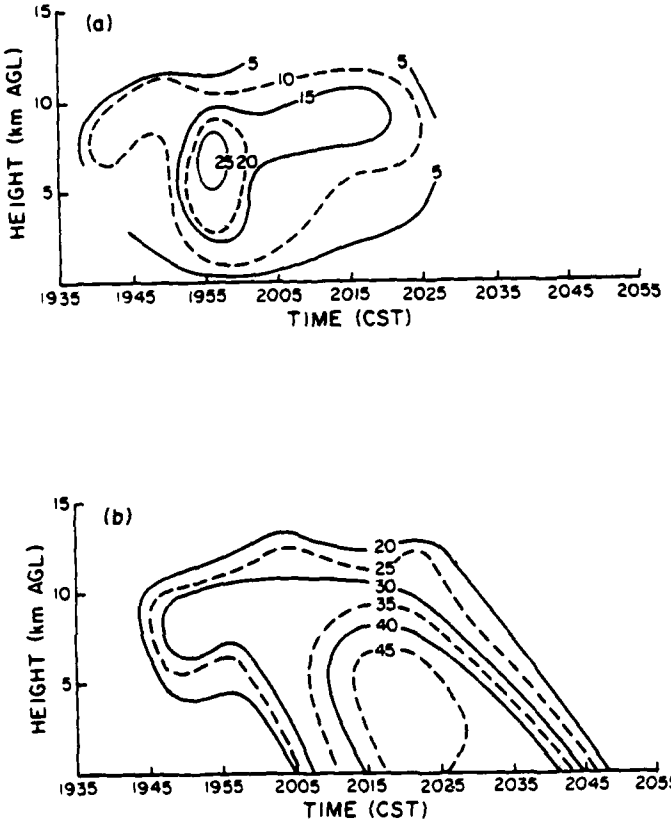

Figure 3 *The evolution of (a) Maximum updraft speed (m s^{-1}), and (b) Maximum reflectivity factor (dBZ) at each altitude in cell C1.*

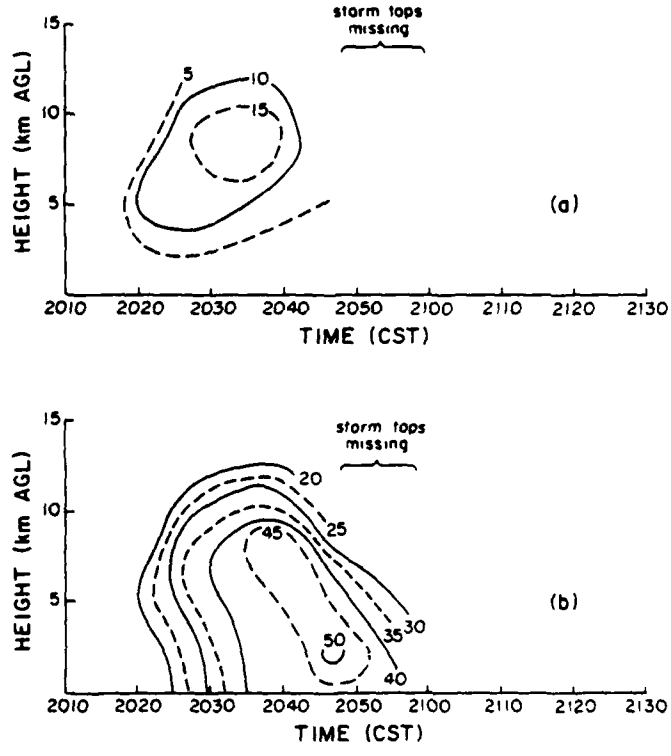

Figure 4 *As in Fig. 3 except for cell C2.*

Figure 4 shows the evolution of maximum reflectivity factor and updraft speed for cell C2. C2 first appeared at ~5 km at about 2020. Peak updraft speeds (~18 m s^{-1}) and maximum height of the cell (~13 km) occurred almost simultaneously; maximum reflectivity (50 dBZ) occurred about 10 minutes later. The maximum reflectivity factor growth rate was ~4 dBZ min^{-1} at middle altitudes in the storm, and the maximum updraft growth rate was ~5 m s^{-1} min^{-1} also at middle altitudes. The life cycle of C2 took place in about 40 minutes.

As seen in Fig. 5, cell C3 became much more intense than C1 or C2. Although data for the central times of the storm's evolution are missing, growth rates can still be determined. The maximum reflectivity factor growth rate was ~7 dBZ min^{-1} at middle altitudes in the storm and the maximum updraft growth rate was ~7 m s^{-1} min^{-1} also at middle altitudes. Maximum reflectivity factor in available data was 57 dBZ (though probably somewhat higher in reality). C3 lasted about 50 minutes.

Cell C4 became more intense than any previous cell (see Fig. 6). Peak updraft speeds exceeded 60 m s^{-1}, maximum cell height exceeded 16 km, and maximum reflectivity factor was at least 60 dBZ. Even though this cell had higher vertical velocities and was much more intense than the others its

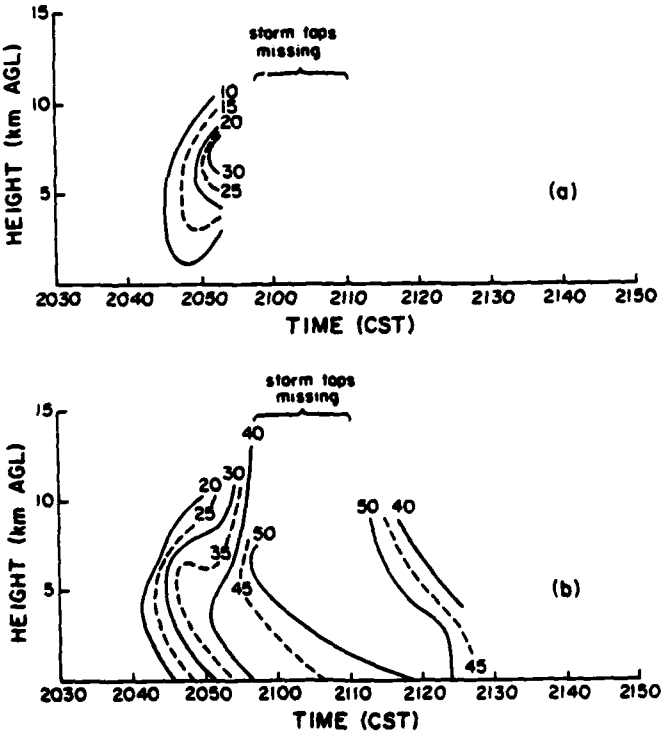

Figure 5 As in Fig. 3 except for cell C3.

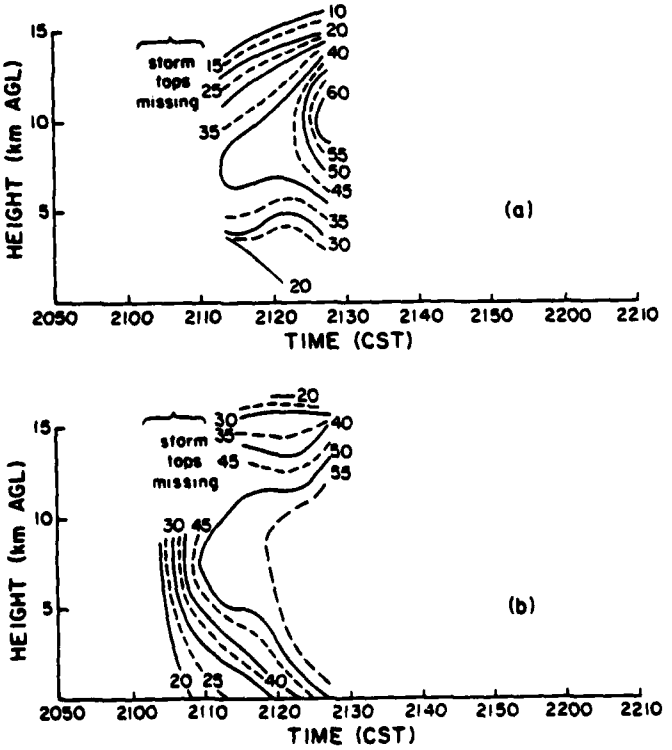

Figure 6 As in Fig. 3 except for cell C4.

maximum reflectivity factor growth rate was only 5 dBZ min^{-1} at middle altitudes of the storm. Because data were not acquired at the storm top during the early evolution of C4, updraft speeds are available only for 2102, the earliest time of cell detection. The next time when vertical motion could be obtained continuously was 2116. The maximum updraft growth rate for the earliest observed data was ~3 m s^{-1} min^{-1}. Note that there was a second surge at upper levels in the vertical motion profile just prior to 2130. The surge had a growth rate of ~5 m s^{-1} min^{-1}.

Subsequent observations revealed that the storm had evolved into a supercell storm where the identification of individual cells was very difficult. However, data from 2153 to 2215 showed that peak updraft speeds were consistently >45 m s^{-1} (often exceeding 60 m s^{-1}) and maximum reflectivity factors were >60 dBZ.

4. EFFECTS OF INTERLACED SCANS ON REAL-TIME ALGORITHMS USED TO TRACK STORM CELLS AND DETERMINE THEIR PARAMETERS

The purpose of this section is to compare computer algorithm performance on data collected in an interlaced scan sequence with performance on data collected in a contiguous scan sequence. A scan sequence is one in which the radar beam sweeps between two azimuth limits (these could be zero and 360° if a full azimuthal circle is scanned) while increasing its elevation angle between ~0° and one that tops the storm. An interlaced sequence is one in which alternate azimuthal sweeps are acquired in two volume scans whereas in the contiguous sequence all sweeps are acquired sequentially in one volume scan. Because Doppler radar antennas at the National Severe Storms Laboratory (NSSL) cannot rotate as rapidly as the proposed NEXRAD system, and in order to compare results obtained from interlaced scans with results from contiguous scans, data used in this study were collected over narrow sectors so that each volume was scanned at twice the proposed NEXRAD rate. Thus, sector volumes with contiguous elevation steps were acquired every 2 1/2 minutes. Alternate scans at constant elevation were deleted from pairs of volume scans to simulate an interlaced-scan pair that would take 5 minutes to acquire (Fig. 7). Data from these pairs, when combined, generated time-lagged, but spatially contiguous, steps in elevation angle. In the volume of interlaced scans, data collected during scans 1, 3, 5, etc., are separated by 2 1/2 minutes from data collected during scans 2, 4, 6, etc., whereas in the proposed NEXRAD data collection procedure, data acquired at contiguous fig 7

elevation steps will have a time separation of about 20 seconds but a repeat cycle of 5 minutes.

Tracking and storm-parameter algorithms were applied to data derived from the simulated interlaced scanning strategy and results were compared to those obtained from the same algorithms applied to data derived from contiguous scans. NSSL's 10 cm Doppler data between 1734 and 1812 CST on 20 May 1982 have been processed with Air Force Geophysics Laboratory (AFGL) algorithms that track storms and estimate storm attributes (e.g., peak reflectivity factor and storm-top altitude). From these data we were able to form interlaced sector volume scans that encompassed a single thunderstorm cell at the beginning, but by the time of the last surveillance the sector contained three storm cells.

The AFGL algorithms locate storm cells according to their 30-dBZ envelope. A minimum scale of 4 km (horizontally) is required before a 30-dBZ

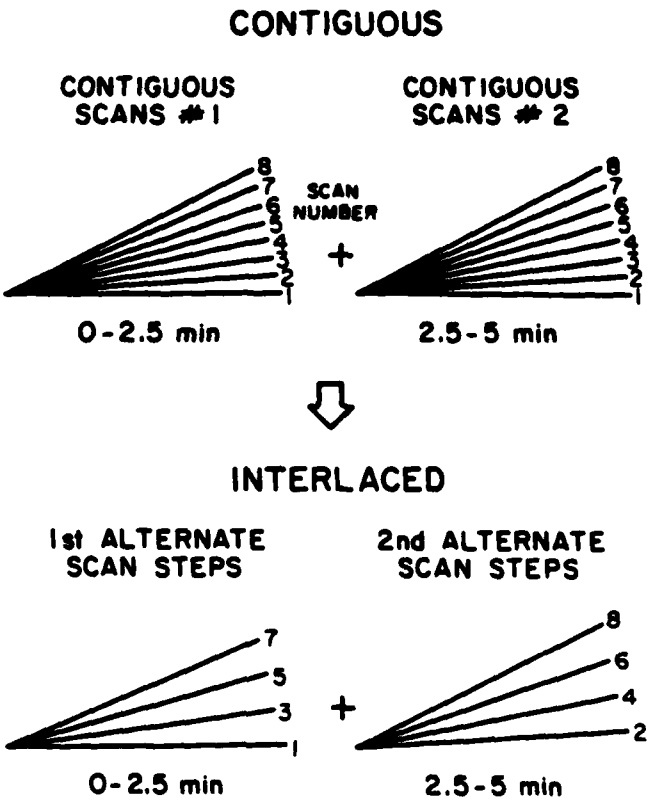

Figure 7 Simulation of interlaced azimuthal scans by deletion of alternate ones at constant elevation from the contiguous set.

envelope is identified as a cell. Furthermore, within certain lateral constraints, a cell must be identified on two successive elevation-angle steps in order to be tracked. Storm cells meeting these criteria are then described by eleven attributes.

Table 1 lists the attribute values for a simulated interlaced scan sequence during the period 1802-1807, bracketed by values for a contiguous scan sequence 2 1/2 minutes earlier and later. The column of data for the period 1802-1805 was obtained from one of the two contiguous scan sequences used to generate the interlaced scan at 1802-1807. The last column lists the differences in attribute values obtained from interlaced and contiguous scans for the time period 1802-1807. The differences between attribute values obtained using interlaced data and those obtained using contiguous data are within the uncertainty and variance that is seen in attribute values from volume scan to volume scan, using contiguous data alone. For example, the speed of storm motion derived from contiguous data changes from 5.8 to 9.7 and then to 15.6 knots over three 5-minute periods, whereas only a 2-knot difference is found when the storm speed derived from interlaced data is compared to the speed derived from contiguous data collected during the same period.

Table 2 lists the differences between results in storm cell attributes for three other periods. Again note the differences between attribute values obtained using the non-interlaced and interlaced scans, and then compare them to the differences in the attribute values for the three non-interlaced scans. The changes over 5-minute intervals observed in the non-interlaced scans are sometimes larger than the differences between interlaced and non-interlaced scans. The most complex algorithm (not shown in tables) is the weighted 7-variable test for the likelihood of hail. Both non-interlaced and interlaced data showed evidence of hail.

5. SUMMARY AND DISCUSSION

Reflectivity factor growth rates calculated for four cells ranged from 4 to 5 dBZ min^{-1}. Maximum reflectivity factors ranged from 50 to >60 dBZ, and maximum cell heights ranged from 13 to >16 km. Updraft growth rates ranged from 3 to 7 m s^{-1} min^{-1}. Peak updraft speeds ranged from 15 m s^{-1} to >60 m s^{-1}. Each cell became more intense than its predecessor while exhibiting similar evolutionary characteristics; peak updrafts occurred

TABLE 1. Storm cell attribute values, and differences between them, for three non-interlaced (N) and one interlaced (I) scanning strategies. Second half of the non-interlaced scan pair for 1802-1807 is not shown. Seconds have been dropped from the times.

	TIME (CST)				
	1757-1801	1802-1805	1802-1807	1807-1810	1802-1807
Attribute	N	N	I	N	N-I
AZM (deg)	248	247	246	249	1
RANGE (nm)	56	53	53	48	0
HT (ft x 1000)	17.1	18.0	17.4	13.5	0.6
BASE (ft x 1000)	-3.6	7.9	7.5	-3.0	0.4
TOP (ft x 1000)	41.0	43.6	42.3	27.2	1.3
MXREF (dBZ)	66	67	68	65	-1
ALT (ft x 1000)	19.7	17.4	17.4	7.5	0
MASS (ktons x 100)	42	51	53	73	-2
VOL (km^3 x 100)	37	43	46	69	-3
SPEED (Kn)	5.8	9.7	11.7	15.6	-2.0
DIR (deg)	294	274	271	258	3

RANGE, AZM, and HT - The 30-dBZ centroid location with respect to the radar.

BASE AND TOP - The bottom and top of the 30-dBZ contour. If these values are negative, the level was the lowest or highest level scanned, and it cannot be established if it was the actual base or top.

MASS - A Mass of the storm within the storm volume (VOL).

VOL - The volume of the storm containing a reflectivity factor of 30 dBZ and greater.

SPEED and DIR - The observed motion of the 30-dBZ contour centroid.

MXREF - The maximum reflectivity factor found in the storm cell.

ALT - The altitude at which MXREF was found.

TABLE 2. Storm cell attribute values and differences between them, for three interlaced (I) and three non-interlaced (N) scanning strategies. Second halves of the non-interlaced scan pairs are not shown. Seconds have been dropped from times.

	TIME (CST)								
	1733 - 1736			1737 - 1740			1742-1745		
Attribute	N	I	N-I	N	I	N-I	N	I	N-I
AZM (deg) 249	249	0	249	249	0	249	248	1	
RANGE (nm) 58	58	0	57	58	-1	59	59	0	
HT (ft x 1000)	11.5	11.8	-0.3	12.1	12.5	-0.4	14.1	14.4	-0.3
BASE (ft x 1000)	-4.3	-4.3	0	-3.9	-3.9	0	-3.9	-3.9	0
TOP (ft x 1000)	35.1	35.1	0	27.9	29.9	-2.0	40.7	40.7	0
MXREF (dBZ)	57	58	-1	57	57	0	57	57	0
ALT (ft x 1000)	9.5	9.5	0	15.1	15.1	0	20.7	20.3	0.4
MASS (ktons x 100)	15	17	-2	16	16	0	17	17	0
VOL (km^3 x 100)	20	21	-1	23	24	-1	26	27	-1
SPEED (Kn) -	-	-	17.5	0	17.5	3.9	1.9	2.0	
DIR (deg) -	-	-	243	270	-27	86	0	86	

~10 minutes before the maximum cell height was attained and as much as 10-20 minutes before maximum reflectivity. There seemed to be no correlation between high reflectivity and updraft growth rates. However, peak updraft speeds, maximum cell heights, and maximum reflectivity appeared to be highly correlated although staggered in time. The cells typically lasted 40 minutes to 1 hour.

Comparison of output from algorithms used to track storm cells and to determine storm cell attributes shows that differences between attribute values derived from interlaced and contiguous scan sequences are about the same as differences between attribute values derived from consecutive contiguous scan sequences. Thus, it appears possible that a radar using interlaced scanning may detect hazards in one-half the time for the proposed NEXRAD contiguous scanning strategy without significant error in storm attribute values (as determined using AFGL algorithms). These results, however, are not entirely conclusive, because of variability in algorithm output (especially in determining storm motion) and the fact that the data base is inadequate for a thorough statistical examination. Further, the necessity of obtaining data at twice the normal rate cannot be substantiated by the results from the growth rate study described in this report. Although some hazardous features (e.g., microbursts) may occur very rapidly, others tend to develop in the time frame of the proposed NEXRAD scanning strategy. For example, a reflectivity growth rate of 7 dBZ min^{-1} (maximum found in this study) would mean that a 65-dBZ echo would be well detected over two 5-minute volume scans. Therefore, we consider that additional research is necessary on the impact that small-scale hazards, shown by Doppler velocity fields, would have on NEXRAD scanning strategies and algorithms.

REFERENCES

McCarthy, J., R. Serafin, 1984: The microburst: Hazard to aviation. **Weatherwise, 37(3)**, pp. 120-127.

Ray, P.S., C.L. Ziegler, W. Bumgarner, R.J. Serafin, 1980: Single- and multiple-Doppler observations of tornadic storms. **Mon. Wea. Rev., 108**, 1607-1625.

JDOP Staff, 1979: Final report on the Joint Doppler Operation Project (JDOP), 1976-1978, NOAA Tech. Memo. ERL NSSL-86, Norman, National Severe Storms Laboratory, 84 pp. (NTIS, PB80-107188/AS).

Vasiloff, S.V., E.A. Brandes, 1984: An investigation of the transition from multicell to supercell storms. **Preprints**, 22nd Conf. on Radar Meteorology, 10-13 Sept. 1984, Amer. Meteor. Soc., Boston, Mass. 02108, 77-82.

Mahapatra, P.R., D.S. Zrnic', R.J. Doviak, 1983: Optimum siting of NEXRAD to detect hazardous weather at airports. **J. Aircraft**, Vol. 20, No. 4, pp. 363-371.

END

FILMED

11-85

DTIC